Inorganic Chemistry

Article

pubs.acs.org/IC

Cis–Trans Isomeric and Polymorphic Effects on the Magnetic Properties of Water-Bridged Copper Coordination Chains

Bojan Kozlevčar,*[,†] Nives Kitanovski,[†] Zvonko Jagličić,[§,‡] Nuno A. G. Bandeira,[∥] Vincent Robert,*[,#,∥] Boris Le Guennic,*[,∥,¶] and Patrick Gamez[⊥]

[†]Fakulteta za kemijo in kemijsko tehnologijo, Univerza v Ljubljani, Aškerčeva c. 5, 1000 Ljubljana, Slovenia

[§]Inštitut za matematiko, fiziko in mehaniko, Jadranska c. 19, 1000 Ljubljana, Slovenia

[‡]Fakulteta za Gradbeništvo in Geodezijo, Univerza v Ljubljani, Jamova c. 2, 1000 Ljubljana, Slovenia

[∥]Laboratoire de Chimie, Ecole Normale Supérieure de Lyon, CNRS, 46 Allée d'Italie 69364 Lyon CEDEX 07 France

[#]Laboratoire de Chimie Quantique, Institut de Chimie UMR 7177, CNRS and Université de Strasbourg, 4 rue Blaise Pascal, 67070 Strasbourg, France

[¶]Institut des Sciences Chimiques de Rennes, UMR 6226 CNRS-Université de Rennes 1, 35042 Rennes, Cedex, France

[⊥]ICREA, Departament de Química Inorgànica QBI, Universitat de Barcelona, Martí i Franquès 1-11, 08028 Barcelona, Spain

Supporting Information

ABSTRACT: The synthesis and magnetic characterization of vanillin-based Cu(II) mononuclear complexes of formula $[Cu(van)_2(H_2O)_2](H_2O)_x$ (**van** = vanillinate; $x = 0$, compound **1**; $x = 2$, compounds **2** and **3**) were performed. Despite the presence of very similar $[Cu(\mathbf{van})_2(H_2O)_2]$ moieties, the crystal structures exhibit distinct Cu···Cu contacts and display three different through-H-bond exchange-coupling pathways. As a result of the relative positions of the water molecules, the experimental (MAGSUS) exchange-coupling constants are dissimilar, i.e., $J(\mathbf{1}) = -3.0$ cm^{-1} (the data have been fitted to the Bleaney–Bowers equation considering a dimer; $2J = -6.0$ cm^{-1}), $J(\mathbf{2}) = -4.0$ cm^{-1} (the data have been fitted to the Bonner–Fischer equation for a chain of monomeric copper(II) units), whereas compound **3** is paramagnetic. Subsequently, the theoretical density functional theory (DFT) and wave function theory-based (DDCI) calculations were carried out to better understand the role of the water molecule as a mediator of the magnetic coupling. The use of localized orbitals allows one to elucidate the role of the H-bonds in generating exchange interactions. Since the exchange-coupling constants are strongly dependent on the mechanisms selectively introduced, the role of the H-bond is demonstrated.

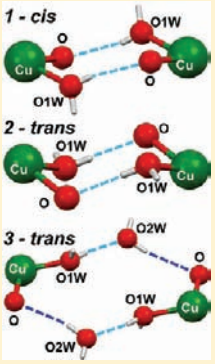

INTRODUCTION

About 70% of the Earth's surface is covered by water,[1] which is crucial in numerous life processes.[2−5] For instance, water is crucial for biological proton-transfer processes,[6−9] and it is found commonly in active sites of metalloenzymes[10,11] where it may act as a bridging ligand between metal ions,[12−14] favoring their magnetic interaction.[15,16]

Water is obviously a good solvent for many natural molecules and is characterized by its marked polarity and tendency to generate hydrogen bonds with a great number of molecules. Hence, the use of potential naturally occurring ligands to bind metal ions in water represents an ideal situation for the (coordination) chemist, both from environmental and economic issues. In that context, during the past five years, some of us were involved in research investigations dedicated to the development of new eco-friendly fungicides for wood preservation that would replace the highly toxic chromium species currently utilized.[17] For that purpose, copper coordination compounds based on a lignin model ligand (to mimic potential copper–lignin interactions), namely vanillin, have been studied.[18−21]

Actually, the reaction of water-soluble vanillin with copper(II) acetate produces three related mononuclear complexes (Scheme 1), whose slight structural disparities are induced by the solvent, i.e., water. Amazingly, these a priori insignificant differences generate noticeable variations of the magnetic interactions between the paramagnetic metal centers. A thorough analysis of the solid-state structures of the three compounds, as well as in-depth theoretical calculations, has been carried out on these three analogous complexes of formula $[Cu(\mathbf{van})_2(H_2O)_2](H_2O)_x$ (**van** = vanillinate; $x = 0$, compound **1**; $x = 2$, compounds **2** and **3**) to better understand the variations of the magnetic properties observed. The present investigation clearly shows that the distinct stereoisomers and hydrogen-bonding networks created by bound and/or lattice water molecules affect the intermolecular exchange pathway between the copper ions in **1**−**3**.

EXPERIMENTAL SECTION

Materials. Complexes $[Cu(\mathbf{van})_2(H_2O)_2]$ (**1**) and $[Cu(\mathbf{van})_2(H_2O)_2](H_2O)_2$ (**2** and **3**) were prepared according to literature methods.[20]

Magnetic Measurements. The magnetic susceptibility data of powdered polycrystalline samples of **1**−**3** were recorded between 2 and 300 K with a Quantum Design MPMS-XL-5 SQUID magnetometer,

Received: November 29, 2011
Published: February 22, 2012

   dx.doi.org/10.1021/ic202568y | *Inorg. Chem.* 2012, 51, 3094−3102

Scheme 1. Synthetic Pathways to Prepare the Related $[Cu(van)_2(H_2O)_2](H_2O)_x$ Compounds 1−3[a,19−21]

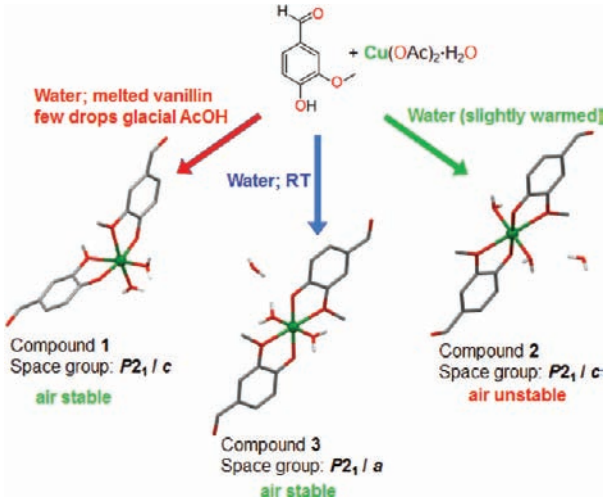

[a] **van** stands for vanillinate; x = 0 for compound **1**, and x = 2 for compounds **2** and **3**.

in a constant magnetic field **H** = 1000 Oe. The data were corrected for the sample holder contribution and for a temperature-independent magnetic susceptibility of inner shell electrons (Larmor diamagnetism), as obtained from Pascal's tables.[22] The magnetic data were fitted using the Heisenberg spin for two isolated interacting copper(II) ions using the Hamiltonian $H = -2J\ S_1 \cdot S_2$, while for the chain the Hamiltonian is $H = -2J\ \Sigma\ S_i \cdot S_{i+1}$; $i = 1 - n$.[22]

Computational Details. Calculations were performed on dinuclear models ensuing from the crystallographic data of complexes **1**−**3**, without any geometry optimization. Density functional theory (DFT) calculations were carried out with the Amsterdam Density Functional (release 2010.01) program.[23] The exchange-coupling parameter J was calculated on the basis of the broken symmetry (BS) method,[24,25] using the nonspin-projected (NSP) expression

$$2J = E(BS) - E(T)$$

where E(BS) and E(T) are the total energies of the broken-symmetry and triplet states, respectively. Even if the use of this expression is still controversial,[26−32] it usually reproduces correctly the experimental values.[33−36] It has to be mentioned that for two magnetic centers with $s_z = 1/2$ such as Cu(II) ions, the spin-projected (SP) form will give a J value twice larger than the corresponding NSP values. Moreover, since the calculated energy difference is strongly related to the nature of the exchange correlation functional,[37−41] the pure GGA (generalized gradient approximation) BP86 functional has been selected,[42] as well as the three-parameter hybrid functional of Becke based on the correlation functional of Lee, Yang, and Parr (B3LYP),[43,44] both employing the default local density functional based on the Vosko-Wilk-Nusair parametrization.[45] Finally, the hybrid meta-GGA M06 functional, developed by Truhlar and co-workers,[46] was used in the present calculations since it has been shown recently that this functional provides excellent agreement between calculated and experimental exchange-coupling constants, as evidenced in a series of dinuclear transition metal complexes.[41,47] Since it was not possible to find a broken symmetry state using the M06 functional using conventional (atomic) fragments, each monomer was considered as a fragment unit and a broken symmetry state was imposed using the FRAGOCCUPATIONS key. All remaining program defaults were applied. Copper atoms were described by triple-ζ uncontracted Slater type basis sets augmented with two polarization p and f functions (TZ2P), whereas double-ζ basis sets augmented with a polarization function (DZP) were used for carbon, oxygen, and hydrogen atoms.

To complement the DFT picture, complete active space self-consistent field (CASSCF)[48] calculations, including two electrons in two molecular orbitals (MOs), were performed with the MOLCAS 7.2 package.[49] In this wave function theory (WFT) scheme, a reference space (CAS[2,2]) is first generated to qualitatively include the relevant electronic configurations. Then, the dynamical correlation effects were incorporated on top of the triplet CASSCF wave function using the dedicated difference configuration interaction (DDCI)[50,51] method implemented in the CASDI code.[52] With this approach, one concentrates on the differential effects rather than on the evaluation of the absolute energies. In order to assess the role played by hydrogen bonding in the spin coupling of these Cu(II) complexes, two computational strategies were adopted for which the CASSCF orbitals were localized to generate a valence bond-type picture of the bonding patterns present in the complexes and to offer a physical analysis.[53] These localized orbitals (LOs) are symmetry adapted (C_i) and orthogonal. Each occupied LO can then be associated with a specific chemical bond. Along this scheme, the water ligand is described by two lone pairs, two bonding σ_{O-H} and two antibonding σ^*_{O-H} LOs. The hydrogen bond involves the electrons of a lone pair localized on a negatively polarized oxygen donor atom (from the phenoxy groups) and a close in space σ^*_{O-H} LO. As previously reported, a concerted step with the metal orbitals may contribute to the overall magnetic exchange coupling.[54] In the first approach, the localized CAS[2,2]SCF MOs of the triplet state were used to evaluate the singlet−triplet energy difference at the DDCI-3 level. The aforementioned contributions arising from the chemically relevant LOs described above are thus not taken into account (see Scheme 2, left). Following a strategy that was

Scheme 2. Various DDCI Approaches Used to Assess the Role of Hydrogen Bonds in the Singlet−Triplet Energy Gap

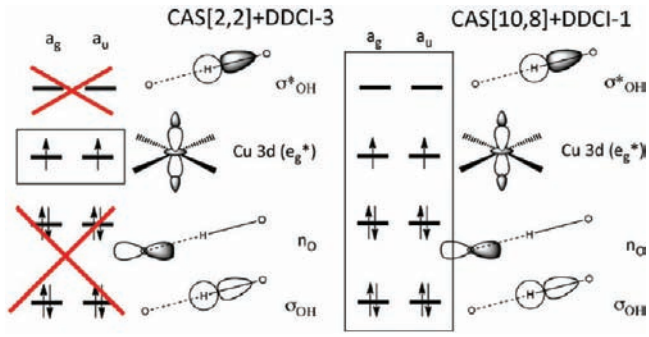

successfully applied in through H-bond spin-coupled Cu(II) centers,[54,55] a 10 electron/8 orbital active space was constructed and the singlet−triplet energy gap was calculated at the CAS[10,8]+DDCI-1 level (see Scheme 2). Along this scheme, the computation of the CAS[10,8]SCF wave function from a localized CAS[2,2] guess favors a lone pair of the H_2O ligand (referred to as CAS[10,8]^{H2O}). This suggests that the presence of this lone pair in the active space brings more static correlation than a lone pair from the phenoxy group. One may also notice that there is a delocalization tail in the σ^*_{O-H} orbital that already contains a small contribution of a phenoxy group oxygen sp lone pair. Therefore, a rotation restriction of the latter via the "supsym" keyword was imposed to maintain the phenoxy group oxygen sp lone pair in the active space (referred to as CAS[10,8]^{O}). Subsequently, the DDCI-1 step was also carried out using this set of orbitals and the J values were extracted.

All atoms were depicted with ANO-RCC type basis sets with the following contraction schemes: (21s15p10d6f4g2h)/[5s4p3d] for copper atoms;[56] (14s9p4d3f2g)/[2s1p] for carbon;[57] (14s9p4d3f2g)/[3s2p1d] for oxygen except for the oxygen belonging to the CHO group which was kept with a valence only 2s1p contraction;[57] Finally, a (8s4p3d1f)/[2s1p] contraction was used for the H atoms involved in the hydrogen bonds, whereas a minimal basis set (8s4p3d1f)/[1s] was used for the other hydrogen atoms.[58]

RESULTS AND DISCUSSION

Description of the Structures. The reaction of an aqueous copper(II) acetate solution with melted vanillin produces a

dx.doi.org/10.1021/ic202568y | Inorg. Chem. 2012, 51, 3094−3102

mononuclear compound, namely *cis*-[Cu(**van**)$_2$(H$_2$O)$_2$] (**1**) (**van** = vanillinate; Scheme 1).[21] The coprecipitation of the complex *trans*-[Cu(**van**)$_2$(H$_2$O)$_2$](H$_2$O)$_2$ (**2**)[20] was prevented by addition of one drop of acetic acid. Pure compound **2** could be isolated when a warmed aqueous solution of copper acetate was added to solid vanillin at room temperature. When the same reaction is carried out carefully at room temperature (without stirring!), *trans*-[Cu(**van**)$_2$(H$_2$O)$_2$](H$_2$O)$_2$ (**3**),[20] a polymorph[59] of **2**, is obtained (Scheme 1). Selected bond distances and angles for these three compounds are listed in Table 1.

Table 1. Selected Bond Distances (Å) and Angles (°) for Compounds 1−3[a,19−21]

		1	
Cu−O1A	2.151(1)	O1A−Cu−O2A	79.31(3)
Cu−O1B	2.354(1)	O2A−Cu−O2W	92.87(3)
Cu−O1W	2.163(1)	O2W−Cu−O2B	94.92(3)
Cu−O2W	2.020(1)	O2B−Cu−O1A	93.00(3)
Cu−O2A	1.920(1)	O1B−Cu−O1W	168.43(3)
Cu−O2B	1.914(1)		
Cu···Cu	5.206(2)		
		2	
Cu−O3	2.327(1)	O3−Cu−O4	76.43(5)
Cu−O4	1.938(1)	O4−Cu−O3a	103.57(5)
Cu−O1W	2.011(1)		
		O1W−Cu−O1Wa	180.00
Cu···Cu	4.904(2) Å		
		3	
Cu−O1	2.327(1)	O1−Cu−O2	76.28(4)
Cu−O2	1.959(1)	O2−Cu−O1a'	103.72(4)
Cu−O1W	1.983(1)		
		O1W−Cu−O1Wa'	180.00
Cu···Cu	6.543(2)		

[a]Symmetry operations: a = −*x*, 1 − *y*, 1 − *z*; a' = 2 − *x*, −*y*, 2 − *z*.

***cis*-[Cu(van)$_2$(H$_2$O)$_2$] (1).** Compound **1** crystallizes in the monoclinic space group $P2_1/c$. The CuO$_6$ octahedral core is formed by four oxygen atoms (O1A, O2A, O1B, and O2B) belonging to two vanillinate ligands and two cis-oriented water molecules (oxygen atoms O1W and O2W).[21] Each coordinated water molecule interacts, through a hydrogen bond, with a phenolato oxygen atom from an adjacent molecule of **1** (blue dotted lines in Figure 1). As a result, each mononuclear unit is

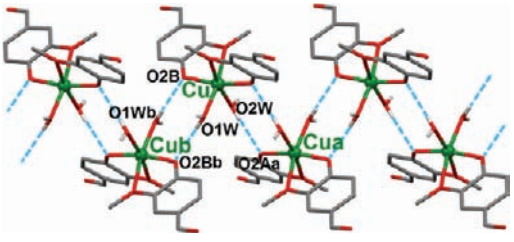

Figure 1. Hydrogen-bonding network (blue dotted lines) involving coordinated vanillinate ligands (phenolato oxygen atoms O2A and O2B) and water molecules (oxygen atoms O1W and O2W), generating a zigzag-type supramolecular chain of **1** (O2W···O2Aa = 2.713(1) and O2B···O1 Wb = 2.767(1) Å; Table 2). Symmetry operations: *a* = −*x*, 1 − *y*, 1 − *z*; *b* = 1 − *x*, 1 − *y*, 1 − *z*.

connected to two neighbors by means of double H-bond bridges (O1W−H2W1···O2Bb = 2.767(1) Å on one side, and double O2W−H2W2···O2Aa = 2.713(1) Å on the other one; Table 2), which produces a zigzag-type supramolecular chain (Figure 1), running along the crystallographic *c* axis. In addition, each one-dimensional (1-D) chain interacts with four adjacent ones via four O$_{water}$−H···O$_{aldehyde}$ bonds (O1W−H1W1···O3Bc = 2.780(1) Å and O2W−H1W2···O3Ad = 2.727(1) Å; Figure 2 left), yielding a 3-D supramolecular framework (Figure 2 right). The shortest intrachain Cu···Cua distance is 5.206(2) Å (and 5.302(2) Å for Cu···Cub), while the interchain one is 7.979(2) Å. Compound **1** may be considered as a hydrogen-bonded chain of alternated Cu···Cua and Cu···Cub dimers.

***trans*-[Cu(van)$_2$(H$_2$O)$_2$](H$_2$O)$_2$ (2).** Compound **2** crystallizes in the monoclinic space group $P2_1/c$.[20] As for compound **1**, the CuO$_6$ octahedral core in **2** contains four vanillinate oxygen atoms (O3, O4, O3a, and O4a; symmetry operation: a = −*x*, 1 − *y*, 1 − *z*) from two ligands and two water molecules (O1W and O1Wa).[20] However, in contrast to **1**, the water molecules are *trans*-coordinated in **2**. Again, these coordinated water molecules are involved in hydrogen-bonding interactions with phenolato oxygen acceptors from neighboring mononuclear units (O1W−H11···O4c = 2.651(2); Table 2). The trans-orientation of the water ligands now gives rise to the formation of a linear supramolecular chain running along the crystallographic *a* axis, built from double H bonds (blue dotted lines in Figure 3). Similarly to **1**, the coordinated water molecules are hydrogen bonded to adjacent aldehydic groups (O1W−H12···O11g = 2.686(2) Å; Table 2 and Figure 4 left), connecting the chains to each other. In addition, the solid-state structure of this trans-isomeric form of the coordination moiety [Cu(**van**)$_2$(H$_2$O)$_2$] exhibits lattice water molecules (oxygen atom O2W) that are hydrogen bonded to each other (O2W−H22···O2 Wb = 2.813(3) Å; Table 2) and to the coordinated water ligands (O2W−H21···O1W = 2.971(2) Å; Table 2 and Figure 4 left). The resulting intricate H-bonding network produces a 3-D supramolecular assembly, displaying zigzag water chains between the linear coordination polymers (Figures S1 (Supporting Information) and 4 right). Consequently, the shortest interchain Cu···Cu distance of 9.479(2) Å in **2** is significantly larger compared to that of **1**, whose chains are more closely packed (see Figures 2 right and 4 right). The shortest intrachain Cu···Cu separation distance is 4.904(2) Å. It should be mentioned that once removed from the mother liquor, compound **2** loses its crystallinity, most likely as the result of the evaporation of the two lattice water molecules, giving *trans*-[Cu(van)$_2$(H$_2$O)$_2$] (**2a**).

***trans*-[Cu(van)$_2$(H$_2$O)$_2$](H$_2$O)$_2$ (3).** Compound **3**, an air-stable polymorph of **2**, crystallizes in the monoclinic space group $P2_1/a$.[21,59] Hence, the CuO$_6$ octahedral core in **3** is very similar to that of **2** (see metric parameters in Table 1), with two trans-coordinated water molecules. Significant differences are observed between **2** and **3** in their respective crystal packing, which arise from distinct interactions (through hydrogen bonds) between the CuO$_6$ coordination units. Contrary to compound **2** (see O1W···O4c contact in Figure 3), in **3**, the coordinated water molecules (oxygen atom O1W; Figure 5) are not directly connected to an adjacent copper(II) moiety through a O$_{water}$−H···O$_{phenolato}$ bond; actually, a lattice water molecule (oxygen atom O2W; Figure 5) is intercalated between two *trans*-[Cu(**van**)$_2$(H$_2$O)$_2$] complexes, whose involvement in H-bonding interactions avoids their loss once the compound is removed from the mother liquor (in contrast to compound **2**; see above). Therefore, the linear Cu···Cu supramolecular chain is now generated by four hydrogen bonds (O2···O2Wi = 2.805(2) Å;

dx.doi.org/10.1021/ic202568y | *Inorg. Chem.* 2012, 51, 3094−3102

Table 2. Hydrogen-Bonding Parameters for Compounds 1−3[a,19−21]

1 (Figures 1 and 2)			
O1Wb−H2W1b···O2B	2.767(1)	O1Wb−H2W1b−O2b	165(1)
O2W−H2W2···O2Aa	2.713(1)	O2W−H2W2−O2Aa	166(2)
O1W−H1W1···O3Bc	2.780(1)	O1W−H1W1−O3Bc	175(1)
O2W−H1W2···O3Ad	2.727(1)	O2W−H1W2−O3Ad	174(1)
2 (Figures 3 and 4)			
O1W−H11···O4c'	2.651(2)	O1W−H11−O4c'	179(4)
O2W−H21···O1W	2.971(2)	O2W−H21−O1W	169(3)
O1W−H12···O11g	2.686(2)	O1W−H12−O11g	174(3)
O2W−H22···O2Wb'	2.813(3)	O2W−H22−O2Wb'	149(6)
3 (Figures 5 and 6)			
O1W−H11···O2W	2.676(2)	O1W−H11−O2W	170(2)
O2W−H20···O2i	2.805(2)	O2W−H20−O2i	173(3)
O1W−H10···Og'	2.730(2)	O1W−H10−Og'	176(3)
O2W−H21···O2j	3.007(2)	O1W−H21−O2j	171(2)

[a]Symmetry operations: a = −*x*, 1 − *y*, 1 − *z*; b = c' = 1 − *x*, 1 − *y*, 1 − *z*; b' = 1 − *x*, 1 − *y*, 2 − *z*; c = *x*, 3/2 − *y*, 1/2 + *z*; d = *x*, 3/2 − *y*, −1/2 + *z*; g = − *x* ,1/2 + *y*, 3/2 − *z*; g' = *x*, *y*, −1 + *z*; i = −1/2 + *x*, 1/2 − *y*, *z*; j = −1 + *x*, *y*, *z*.

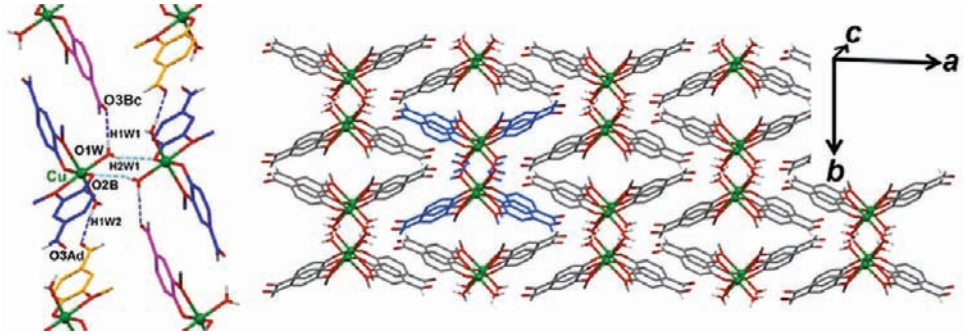

Figure 2. Crystal packing of **1** showing the hydrogen-bonding network (dark-blue dotted lines in the left picture; O3Bc···H1W1 = 1.84(1) Å, O3Ad···H1W2 = 1.77(1) Å; Table 2) that links each zigzag supramolecular chain (one chain is depicted in blue in the right picture) to four adjacent ones, producing a three-dimensional (3-D) architecture. Symmetry operations: *c* = *x*, 3/2 − *y*, 1/2 + *z*; *d* = *x*, 3/2 − *y*, −1/2 + *z*.

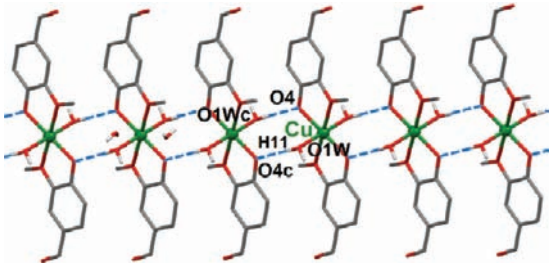

Figure 3. Hydrogen-bonding network (blue dotted lines) involving coordinated vanillinate ligands (phenolato oxygen atom O4) and water molecules (oxygen atom O1W), generating a linear supramolecular chain of **2** (O4···O1Wc = 2.651(2) Å; Table 2). Symmetry operation: *c*, 1 − *x*, 1 − *y*, 1 − *z*.

O1W···O2W = 2.676(2) Å; Table 2). This additional water H-bond increases notably the intrachain Cu···Cu separation distance that amounts to 7.226(2) Å, while it is 4.904(2) Å for **2** and 5.206(2) Å for **1**, for which the supramolecular association of the $[Cu(\mathbf{van})_2(H_2O)_2]$ units is similar to that of **1** (see Figures 1 and 3). As for **2**, the coordinated (O1W) and lattice (O2W) water molecules are involved in hydrogen-bonding interactions (O1W···Og' = 2.730(2) and Å O2W···O2j = 3.007(2) Å; Figure 6 left) with neighboring chains, generating a supramolecular 3-D framework (Figure 6 right), whose shortest interchain Cu···Cu distance is 6.543(2) Å.

Magnetic Properties. As described above, the three copper-vanillinate complexes exhibit significantly different packing features, which are obviously induced by water molecules (cis−trans isomerism or polymorphism). Amazingly, the solid-state structures of compounds **1**−**3**, which contain very similar $[Cu(\mathbf{van})_2(H_2O)_2]$ moieties, reveal distinct Cu···Cu contacts, as is evidenced in Figure 7. The three different through-H-bond exchange-coupling pathways will most likely lead to distinct magnetic properties. We[55,60] and others[61−63] have been involved in the study of magnetic interactions involving neutral water molecules. Hence, the present copper-vanillinate-water system represents a very interesting case in this area of investigation. Therefore, temperature-dependent magnetic susceptibility measurements have been performed for the three compounds (Figure 8).

Compounds **1** and **2** exhibit similar paramagnetic behaviors in the high-temperature region, with $\chi_M T$ values at 300 K of 0.45 and 0.40 cm^3 K/mol, respectively. The corresponding effective magnetic moments μ_{eff} = 1.9 μ_B and 1.8 μ_B were calculated using the formula $\mu_{eff}/\mu_B \cong (8\chi_M T)^{1/2}$.[22] These values are in agreement with that expected for an $S = 1/2$ Cu^{II} ion. The $\chi_M T$ products decrease with the temperature, while χ_M reaches a maximum at about 10 K for both compounds. These features clearly evidence the occurrence of antiferromagnetic interactions in **1** and **2**.

Considering the respective molecular structures of **1** and **2**, two models (i.e., respectively, for a dimer and for a chain) were

dx.doi.org/10.1021/ic202568y | Inorg. Chem. 2012, 51, 3094−3102

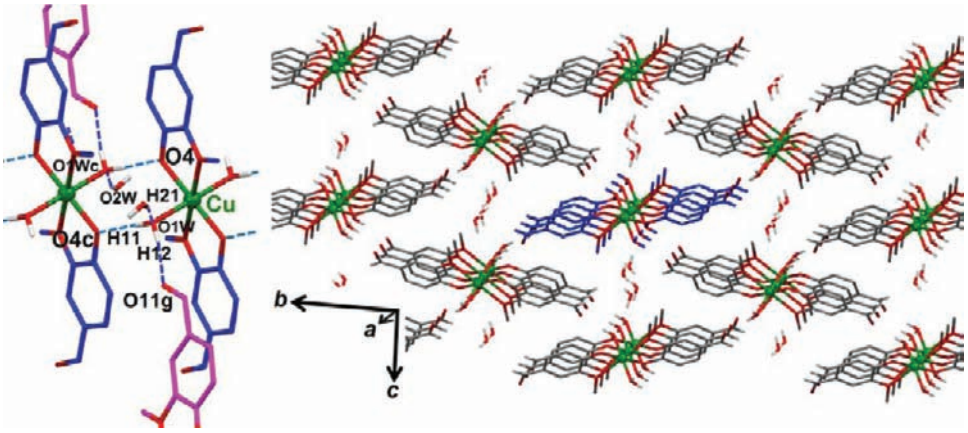

Figure 4. Crystal packing of **2** showing the hydrogen-bonding network (dark-blue dotted lines in the left picture; O11g···H12 = 1.90(3) Å and O1W···H21 = 2.19(3) Å; Table 2) that links each linear supramolecular chain (one chain is depicted in blue in the right picture) to six adjacent ones, producing a 3-D architecture. Symmetry operations: $c = 1 - x, 1 - y, 1 - z$; $g = -x, 1/2 + y, 3/2 - z$.

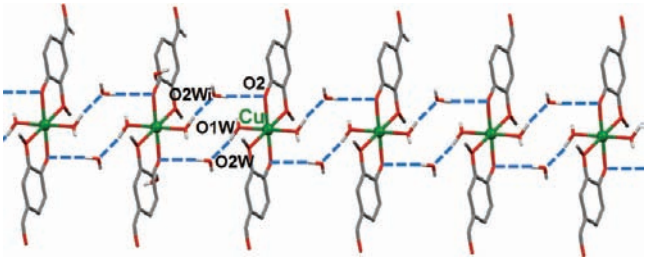

Figure 5. Hydrogen-bonding network (blue dotted lines) involving coordinated vanillinate ligands (phenolato oxygen atom O2) and water molecules (oxygen atoms O1W and O2W), generating a linear supramolecular chain of **3** (O2i···O2W = 2.805(2) Å; O1W···O2W = 2.676(2) Å; Table 2). Symmetry operation: $i = -1/2 + x, 1/2 - y, z$.

used to describe the corresponding temperature-dependent magnetic susceptibility behavior.

Hence, the Bleaney–Bowers eq 1 describes the susceptibility of dinuclear $S = 1/2$ units:[22]

$$\chi_M = \frac{1}{2}\left[(1-\rho)\frac{2N_A g^2 \mu_B{}^2}{k_B T(3 + e^{-2J/k_B T})} + \rho\frac{N_A g^2 \mu_B{}^2}{4k_B T}\right] \quad (1)$$

while the Bonner–Fisher model (eq 2) accounts for infinite chains of $S = 1/2$ spins:

$$\chi_M = (1-\rho)\frac{N_A g^2 \mu_B{}^2}{k_B T}\frac{0.25 + 0.14995x + 0.30094x^2}{1.0 + 1.9862x + 0.68854x^2 + 6.0626x^3} + \rho\frac{N_A g^2 \mu_B{}^2}{4k_B T} \quad (2)$$

In both equations, the second term represents paramagnetic impurities and the factor ρ is the molar fraction of these paramagnetic moments, μ_B the Bohr magneton and k_B the Boltzmann constant. Finally, in eq 2, $x = |J|/T$ where the magnetic spin exchange interaction J (in kelvins) is negative for antiferromagnetically coupled magnetic moments. For compound **1**, the best fit was obtained using the Bleaney–Bowers eq 1 with the exchange interaction $J = -4.3$ K (-3.0 cm^{-1}), $g = 2.2$, and $\rho = 1.1\%$; actually, the use of Bonner–Fischer equation that is commonly applied for a chain did not lead to satisfactory results. On the other hand, for compound **2**, the best fit was achieved with the Bonner–Fisher model (eq 2), with the spin exchange interaction $J = -5.7$ K (-4.0 cm^{-1}), $g = 2.1$, and $\rho = 2.1\%$. In that case, fitting the data with the Bleaney–Bowers equation was not adequate.

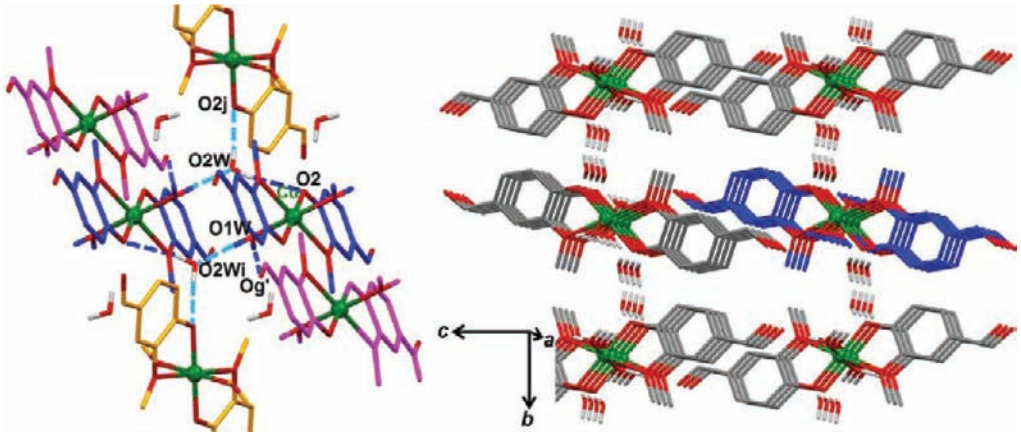

Figure 6. Crystal packing of **3** showing the hydrogen-bonding network (blue dotted lines in the left picture; O2W···O2j = 3.007(2) Å and O1W···Og' = 2.730(2) Å; Table 2) that links each linear supramolecular chain (one chain is depicted in blue in the right picture) to four adjacent ones, producing a 3-D architecture. Symmetry operations: $j = 1/2 + x, 1/2 - y, z$; $g' = x, y, -1 + z$.

dx.doi.org/10.1021/ic202568y | Inorg. Chem. 2012, 51, 3094–3102

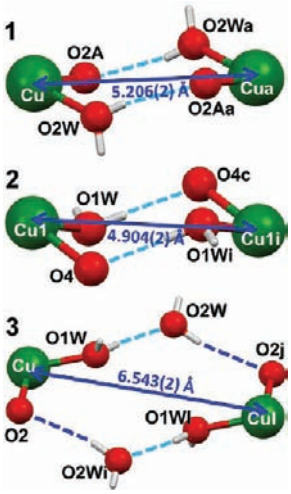

Figure 7. Shortest intrachain metal−metal separation distances for the (water) hydrogen-bonded dicopper(II) units in Å)compound **1** (Cu···Cua =5.206(2) Å), compound **2** (Cu1···Cu1i = 4.904(2) Å), and compound **3** (Cu···CuI =6.543(2) Å). Symmetry operations: $a = -x$, $1 - y$, $1 - z$; $c = 1 - x$, $1 - y$, $1 - z$; $j = -1 + x$, y, z.

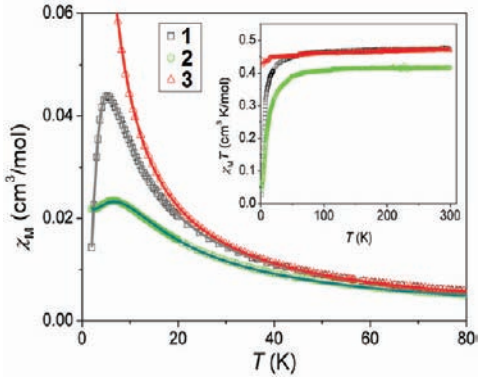

Figure 8. χ_M versus T and $\chi_M T$ versus T plots (inset) for compounds **1**−**3**, χ_M being the molar magnetic susceptibility. Full lines are the best fits to the adequate model (see text).

The susceptibility χ_M of compound **3** increases as the temperature decreases from 300 to 2 K. The product $\chi_M T$ of **3** (inset in Figure 8) is temperature independent, therefore indicating a paramagnetic behavior in all of the temperature range investigated. The susceptibility was successfully described applying the Curie−Weiss law:

$$\chi_M = C/(T - \theta) \qquad (3)$$

The best fit (full red line in Figure 8) was obtained with the Curie constant $C = 0.45$ cm^3 K/mol and the negligible Curie−Weiss temperature $\theta = -0.2$ K. From the Curie constant C, an effective magnetic moment $\mu_{eff} = 1.9\ \mu_B$ per Cu(II) ion was calculated, which corresponds to the expected value for noninteracting Cu(II) ions ($S = 1/2$, $g = 2.2$).[64]

Computational Studies. To further investigate the magnetic properties of compounds **1**−**3**, quantum chemical calculations based on both DFT and CI methodologies (see Computational Details) were performed on dinuclear units extracted from the crystallographic data (Figure 9). Since complex **1** presents two different intrachain Cu···Cu distances, two models, namely, **1a** and **1b**, were constructed on the basis of the Cu···Cua (5.206 Å) and Cu···Cub (5.302 Å) distances, respectively. With the presence of a single intramolecular Cu···Cu distance, complex **2** was modeled only by one dinuclear unit where the Cu(II) ions are separated by a distance of 4.904 Å, which is slightly shorter compared with that in **1**. As mentioned above, the crystal structures of the polymorphic compounds **2** and **3** exhibit significant differences. Indeed, two lattice water molecules are intercalated between adjacent copper moieties in **3**, therefore enlarging the metal−metal distance (6.543 Å in **3** and 4.904 Å in **2**). The influence of these water molecules on the magnetic-exchange channels was thus investigated by keeping (model **3w**) or removing (model **3**) them in the calculations.

First, DFT calculations were performed on all dinuclear models (Figure 9) using various exchange-correlation functionals to preclude any bias due to the choice of potential (see Computational Details). With all the functionals applied, the calculations well reproduce the noninteracting Cu(II) ions in **3** with insignificant computed J values (Table 3). As expected, the BP86 functional overestimates the antiferromagnetic behavior in **1** and **2**, whereas B3LYP and M06 perform similarly, as already stated in the literature.[47,55] A good agreement between the B3LYP (or M06) calculated J value and the experimental data is obtained for complex **2**. For complex **1**, the computed J values for models **1a** and **1b** are both slightly antiferromagnetic and suggest that the main exchange pathway occurs between the Cu and Cua ions (model **1a**), i.e., along the shortest metal−metal distance. Moreover, these results support the involvement of dinuclear $S = 1/2$ units as suggested by the magnetic susceptibility plot obtained from the Bleaney−Bowers equation (Figure 8).

To further investigate the role of hydrogen bonds (water molecules) in the magnetic behaviors of all three materials, CAS[2,2] calculations were performed on the same dinuclear units (Figure 9). For all molecules, the small (or nil) magnetic interaction originates from the weak overlap between the magnetic orbitals. As expected, these orbitals are the combinations of Cu d-type orbitals with small delocalization on the equatorial ligands. As an example, the magnetic orbitals of model **2** are sketched in Figure 10 (see Figure S2 (Supporting Information) for the magnetic orbitals of the other dinuclear units). At the highest level of calculation, i.e., CAS[2,2]+DDCI-3, the calculated exchange-coupling constant is -2.2 cm^{-1} and -0.4 cm^{-1} for complexes **1a** and **1b**, respectively (Table 3). In agreement with the DFT results (B3LYP or M06), these data support a dinuclear description of the magnetic properties of complex **1**. The CAS[2,2]+DDCI-3 J value also supports the small antiferromagnetic behavior of complex **2**.

One may take advantage of orthogonal LOs that were constructed from the CASSCF orbitals (see Computational Details) to assess the participation of hydrogen bonds in the magnetic behavior of both complexes. Indeed, specific mechanisms can be turned on along this strategy, and their relative impacts on the exchange coupling constants can be evaluated. These LOs allow for a chemically intuitive analysis of the relevant mechanisms accompanying the singlet−triplet hierarchization. Using these LOs, a first strategy consists of removing (freezing occupied LOs and deleting vacant LOs) these orbitals in the CAS[2,2]+DDCI-3 calculations (see Table 3). Whereas for complex **2** the computed J value remains the same with and without the presence of H-bonding LOs in the calculation, the situation is different for system **1**, with about 50% difference between both results. A second approach consists of enlarging

dx.doi.org/10.1021/ic202568y | Inorg. Chem. 2012, 51, 3094−3102

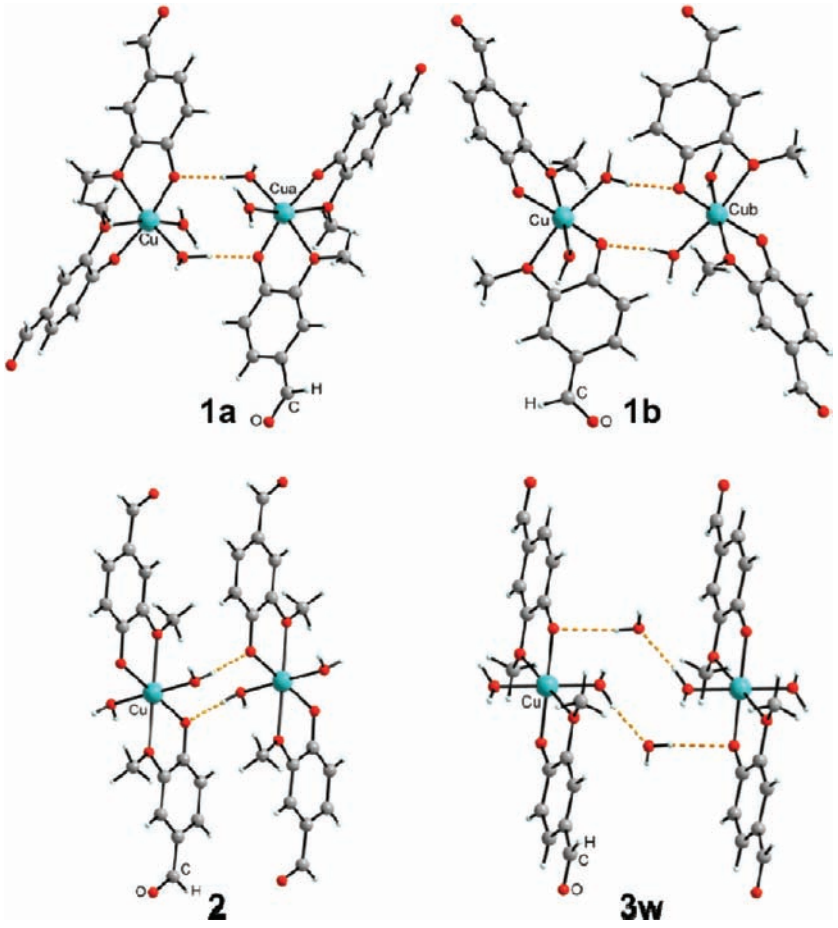

Figure 9. Dinuclear models used in the DFT and WFT (CI) calculations.

Table 3. Calculated Exchange Coupling Constant (J, in cm^{-1}) for the Dinuclear Models of Complexes 1−3, Using Various DFT or CI Computational Strategies

	1			
	1a	1b	2	3 (3w)[b]
DFT (BP86)	−10.8	−1.2	−12.5	+0.1 (0.0)[b]
DFT (B3LYP)	−2.6	−0.3	−2.1	+0.1 (+0.1)[b]
DFT (M06)	−2.3	−0.7	−2.4	+0.2 (+0.1)[b]
CAS[2,2]+DDCI-1	−0.4	0.0	−0.3	0.0 (0.0)[b]
CAS[2,2]+DDCI-3	−2.2 (−1.2)[a]	−0.4 (−0.2)[a]	−3.7 (−3.7)[a]	+2.1 (−0.2)[b]
CAS[10,8]^{H2O}+DDCI-1	+2.0	−7.6	+11.2	
CAS[10,8]^{O}+DDCI-1	+3.6	+14.9	+7.1	
exp.	−3.0	−4.0		

[a]Exchange-coupling constants calculated with freezing the σ_{O-H} bond and the lone pair on the opposite oxygen atom and deleting the σ^*_{O-H} LO. [b]Exchange-coupling constants calculated with the hydrated model **3w** (Figure 9).

the active space in order to include as much information as possible from the hydrogen-bond backbone (CAS[10,8]).[54,55] Using the flexibility offered by the CASSCF procedure, we were able to converge to various CAS[10,8]SCF solutions close enough in energy, depending on the lone pair included in the active space in addition to the Cu d-type orbitals, σ and σ^* orbitals localized on the O−H bond (CAS[10,8]^{H20} vs CAS-[10,8]^{O}; see Figure 11). Whatever the nature of the lone pair, the computed CAS[10,8]+DDCI-1 values significantly differ from those obtained using the canonical CAS[2,2]+DDCI-3 approach, again indicating the essential role that water molecules may play in the magnetic-exchange mechanisms. In view of the interpretative limitations due to the small J values, one may suggest that the inclusion in the active space of the lone pair centered on the phenoxy-type oxygen atom (CAS[10,8]^{O}+DDCI-1) favors ferromagnetic mechanisms for both models **1** and **2** (see Table 3), whereas the circumstances are not as clear when the lone pair on the water ligand is included (CAS-[10,8]^{H2O}+DDCI-1). The origin of such erratic behavior may be explained by the different orientations of the water molecules in structures **1** and **2**. A correct description of the entire mechanism may thus necessitate one to include the whole set of water LOs in the active space. This would be

dx.doi.org/10.1021/ic202568y | Inorg. Chem. 2012, 51, 3094−3102

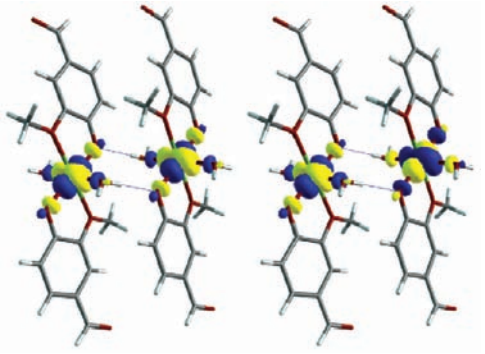

Figure 10. Magnetic MOs resulting from the CAS[2,2]SCF calculations performed on the triplet state of the dinuclear model **2**. MOs for the other dinuclear models are given in the Supporting Information.

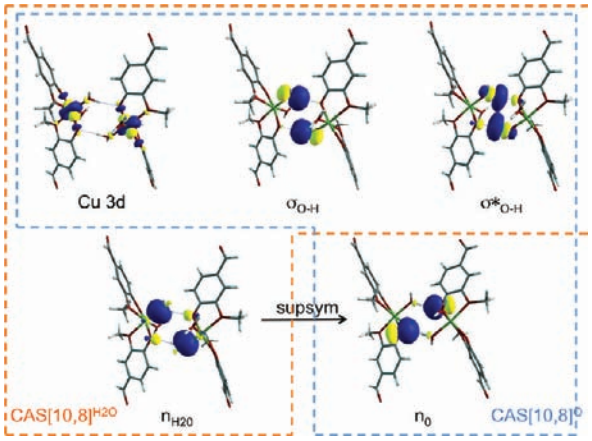

Figure 11. CAS[10,8]SCF triplet MOs of the dinuclear model **1a**. Only the orbitals of a_g symmetry are shown.

the subject of further investigations that are out of the scope of the present work.

For complex **3**, the role of the lattice water molecules (see Figure 7C) was inspected by calculating the exchange-coupling constant with (model **3w**) and without (model **3**) these water molecules. It is interesting to note that, without such extra water molecules, a ferromagnetic behavior is expected from the calculations, in contradiction with the experimental data. However, when the noncoordinated water molecules are taken into account in the calculation, the experimental behavior is recovered with $J(\mathbf{3w}) = -0.2$ cm^{-1}. This result strongly highlights the importance of the cocrystallized water molecules for the magnetic-exchange pathway.

CONCLUSIONS

The combination of experimental and theoretical examinations has provided some insights into the role played by water molecules in exchange-coupled systems. From magnetic susceptibility measurements, the exchange-coupling constants are rather sensitive to the relative positions of the water molecules with respect to the spin carriers. DFT and WFT calculations have been performed to disentangle the effective role played by the bridging molecules. Although the experimental and theoretical results do not perfectly match, not only the amplitude but also the nature of the interactions is deeply modified by the selective insertion of some particular mechanisms in the calculations. Indeed, depending on the number of LOs (i.e., active space enlargement) or nature of the interacting moiety (phenoxy vs water molecule lone pair) considered, variations of ca. 22.5 cm^{-1} are obtained, which reveal that the contribution of the H-bonds in mediating exchange interactions cannot be neglected. This thorough study clearly evidences the particular (important) role of H-bond networks in spin-coupled systems.

ASSOCIATED CONTENT

Supporting Information

Figure S1 illustrating the crystal packing of **2** and Figure S2 illustrating the magnetic molecular orbitals of dinuclear models **1a**, **1b**, **3**, and **3w**. This material is available free of charge via the Internet at http://pubs.acs.org.

AUTHOR INFORMATION

Corresponding Author

*E-mail: Bojan.Kozlevcar@fkkt.uni-lj.si (B.K.); vrobert@unistra.fr (V.R.); boris.leguennic@univ-rennes1.fr (B.L.G.).

Notes

The authors declare no competing financial interest.

ACKNOWLEDGMENTS

P.G. acknowledges ICREA (Institució Catalana de Recerca i Estudis Avançats) and B.K. thanks the ARRS (Javna agencija za raziskovalno dejavnost Republike Slovenije; P1-0175). B.L.G., V.R., and N.A.G.B. thank the ANR project "fdp magnets" for financial support and the Pôle Scientifique de Modélisation Numérique (PSMN) at ENS de Lyon for computing facilities.

REFERENCES

(1) Berner, E. K.; Berner, R. A. *Global Environment: Water, Air, and Geochemical cycles*; Prentice Hall: Upper Saddle River, N.J., 1996.
(2) Stillinger, F. H. *Science* **1980**, *209*, 451−457.
(3) Barron, L. D.; Hecht, L.; Wilson, G. *Biochemistry* **1997**, *36*, 13143−13147.
(4) Jeffrey, J. A.; Saenger, W. *Hydrogen Bonding in Biological Structures*; Springer: Berlin, 1991.
(5) *Water: A Comprehensive Treatise*; Franks, F., Ed.; Plenum: New York, 1972−1982; Vol. *1*−*7*.
(6) Voth, G. A. *Acc. Chem. Res.* **2006**, *39*, 143−150.
(7) Meyer, T. J.; Huynh, M. H. V.; Thorp, H. H. *Angew. Chem., Int. Ed.* **2007**, *46*, 5284−5304.
(8) Bento, I.; Silva, C. S.; Chen, Z. J.; Martins, L. O.; Lindley, P. F.; Soares, C. M. *BMC Struct. Biol.* **2010**, *10*, 28.
(9) Smedarchina, Z.; Siebrand, W.; Fernandez-Ramos, A.; Cui, Q. *J. Am. Chem. Soc.* **2003**, *125*, 243−251.
(10) Yoon, J.; Liboiron, B. D.; Sarangi, R.; Hodgson, K. O.; Hedman, B.; Solomona, E. I *Proc. Natl. Acad. Sci. U. S. A.* **2007**, *104*, 13609−13614.
(11) Maret, W.; Li, Y. *Chem. Rev.* **2009**, *109*, 4682−4707.
(12) Merkx, M.; Kopp, D. A.; Sazinsky, M. H.; Blazyk, J. L.; Muller, J.; Lippard, S. J. *Angew. Chem., Int. Ed.* **2001**, *40*, 2782−2807.
(13) Matoba, Y.; Kumagai, T.; Yamamoto, A.; Yoshitsu, H.; Sugiyama, M. *J. Biol. Chem.* **2006**, *281*, 8981−8990.
(14) Benini, S.; Rypniewski, W. R.; Wilson, K. S.; Miletti, S.; Ciurli, S.; Mangani, S. *Struct. Fold. Des.* **1999**, *7*, 205−216.
(15) Clark, P. A.; Wilcox, D. E. *Inorg. Chem.* **1989**, *28*, 1326−1333.
(16) Samples, C. R.; Howard, T.; Raushel, F. M.; DeRose, V. J. *Biochemistry* **2005**, *44*, 11005−11013.
(17) Kitanovski, N.; Pevec, A.; Kozlevčar, B. *Polyhedron* **2009**, *28*, 3642−3646.
(18) Kozlevčar, B.; Baskovič, P.; Arko, A.; Golobič, A.; Kitanovski, N.; Šegedin, P. *Z. Naturforsch., B* **2008**, *63*, 481−488.

(19) Kozlevčar, B.; Golobič, A.; Strauch, P. *Polyhedron* **2006**, *25*, 2824−2828.
(20) Kozlevčar, B.; Mušič, B.; Lah, N.; Leban, I.; Šegedin, P. *Acta Chim. Slov.* **2005**, *52*, 40−43.
(21) Kozlevčar, B.; Humar, M.; Strauch, P.; Leban, I. *Z. Naturforsch., B* **2005**, *60*, 1273−1277.
(22) Kahn, O. *Molecular Magnetism*; VCH Publishers: New York, 1993.
(23) Baerends, E. J.; Autschbach, J.; Bérces, A.; Bo, C.; Boerrigter, P. M.; Cavallo, L.; Chong, D. P.; Deng, L.; Dickson, R. M.; Ellis, D. E.; v. Faassen, M.; Fan, L.; Fischer, T. H.; Guerra, C. F.; v. Gisbergen, S. J. A.; Groeneveld, J. A.; Gritsenko, O. V.;Grüning, M.; Harris, F. E.; v. d. Hoek, P.; Jacobsen, H.; Jensen, L.; v. Kessel, G.; Kootstra, F.; v. Lenthe, E.; McCormack, D. A.; Michalak, A.; Osinga, V. P.; Patchkovskii, S.; Philipsen, P. H. T.; Post, D.; Pye, C. C.; Ravenek, W.; Ros, P.; Schipper, P. R. T.; Schreckenbach, G.; Snijders, J. G.; Sola, M.; Swart, M.; Swerhone, D.; t. Velde, G.; Vernooijs, P.; Versluis, L.; Visser, O.; Wang, F.; v. Wezenbeek, E.; Wiesenekker, G.; Wolff, S. K.; Woo, T. K.; Yakovlev, A. L.; Ziegler, T. *Scientific Computing and Modelling*, 2010; http://www.scm.com.
(24) Noodleman, L.; Norman, J. G. *J. Chem. Phys.* **1979**, *70*, 4903−4906.
(25) Noodleman, L. *J. Chem. Phys.* **1981**, *74*, 5737−5743.
(26) Ruiz, E.; Cano, J.; Alvarez, S.; Alemany, P. *J. Comput. Chem.* **1999**, *20*, 1391−1400.
(27) Caballol, R.; Castell, O.; Illas, F.; de P. R. Moreira, I.; Malrieu, J. P. *J. Phys. Chem. A* **1997**, *101*, 7860−7866.
(28) Moreira, I. P. R; Illas, F. *Phys. Chem. Chem. Phys.* **2006**, *8*, 1645−1659.
(29) Ruiz, E.; Cano, J.; Alvarez, S.; Polo, V. *J. Chem. Phys.* **2006**, *124*, 107102.
(30) Adamo, C.; Barone, V.; Bencini, A.; Broer, R.; Filatov, M.; Harrison, N. M.; Illas, F.; Malrieu, J. P.; de P. R. Moreira, I. *J. Chem. Phys.* **2006**, *124*, 107101.
(31) Illas, F.; de P. R. Moreira, I.; de Graaf, C.; Barone, V. *Theor. Chem. Acc.* **2000**, *104*, 265−272.
(32) Onofrio, N.; Mouesca, J. M. *Inorg. Chem.* **2011**, *50*, 5577−5586.
(33) Ruiz, E.; Alemany, P.; Alvarez, S.; Cano, J. *J. Am. Chem. Soc.* **1997**, *119*, 1297−1303.
(34) Ruiz, E.; Alvarez, S.; Rodríguez-Fortea, A.; Alemany, P.; Pouillon, Y.; Massobrio, C. *Magnetism: Molecules to Materials*; Wiley-VCH: Weinheim, 2001; Vol. 2, p 227.
(35) Ruiz, E.; Alvarez, S.; Cano, J.; Polo, V. *J. Chem. Phys.* **2005**, *123*, 164110.
(36) Desplanches, C.; Ruiz, E.; Rodriguez-Fortea, A.; Alvarez, S. *J. Am. Chem. Soc.* **2002**, *124*, 5197−5205.
(37) Phillips, J. J.; Peralta, J. E. *J. Chem. Phys.* **2010**, *134*, 034108.
(38) Ruiz, E. *J. Comput. Chem.* **2011**, *32*, 1998−2004.
(39) Peralta, J. E.; Melo, J. I. *J. Chem. Theory Comput.* **2010**, *6*, 1894−1899.
(40) Schwabe, T.; Grimme, S. *J. Phys. Chem. Lett.* **2010**, *1*, 1201−1204.
(41) Valero, R.; Costa, R.; de P. R. Moreira, I.; Truhlar, D. G.; Illas, F. *J. Chem. Phys.* **2008**, *128*, 114103.
(42) Becke, A. D. *Phys. Rev. A* **1988**, *38*, 3098−3100.
(43) Lee, C. T.; Yang, W. T.; Parr, R. G. *Phys. Rev. B* **1988**, *37*, 785−789.
(44) Becke, A. D. *J. Chem. Phys.* **1993**, *98*, 5648−5652.
(45) Vosko, S. H.; Wilk, L.; Nusair, M. *Can. J. Phys.* **1980**, *58*, 1200−1211.
(46) Zhao, Y.; Truhlar, D. G. *Theor. Chem. Acc.* **2008**, *120*, 215−241.
(47) Ruiz, E. *Chem. Phys. Lett.* **2008**, *460*, 336−338.
(48) Roos, B. O. *Adv. Chem. Phys.* **1987**, *69*, 399−445.
(49) Aquilante, F.; De Vico, L.; Ferre, N.; Ghigo, G.; Malmqvist, P. A.; Neogrady, P.; Pedersen, T. B.; Pitonak, M.; Reiher, M.; Roos, B. O.; Serrano-Andres, L.; Urban, M.; Veryazov, V.; Lindh, R. *J. Comput. Chem.* **2010**, *31*, 224−247.
(50) Miralles, J.; Daudey, J. P.; Caballol, R. *Chem. Phys. Lett.* **1992**, *198*, 555−562.
(51) Miralles, J.; Castell, O.; Caballol, R.; Malrieu, J. P. *Chem. Phys.* **1993**, *172*, 33−43.
(52) Ben Amor, N.; Maynau, D. *Chem. Phys. Lett.* **1998**, *286*, 211−220.
(53) Ma, Y.; Bandeiera, N. A. G.; Robert, V.; Gao, E.-Q. *Chem.—Eur. J.* **2011**, *17*, 1988−1998.
(54) Le Guennic, B.; Ben Amor, N.; Maynau, D.; Robert, V. *J. Chem. Theory Comput.* **2009**, *5*, 1506−1510.
(55) Costa, J. S.; Bandeira, N. A. G.; Le Guennic, B.; Robert, V.; Gamez, P.; Chastanet, G.; Ortiz-Frade, L.; Gasque, L. *Inorg. Chem.* **2011**, *50*, 5696−5705.
(56) Roos, B. O.; Lindh, R.; Malmqvist, P. A.; Veryazov, V.; Widmark, P. O. *J. Phys. Chem. A* **2005**, *109*, 6575−6579.
(57) Roos, B. O.; Lindh, R.; Malmqvist, P. A.; Veryazov, V.; Widmark, P. O. *J. Phys. Chem. A* **2004**, *108*, 2851−2858.
(58) Widmark, P. O.; Malmqvist, P. A.; Roos, B. O. *Theor. Chim. Acta* **1990**, *77*, 291−306.
(59) Bernstein, J. *Cryst. Growth Des.* **2011**, *11*, 632−650.
(60) Tang, J. K.; Costa, J. S.; Golobič, A.; Kozlevčar, B.; Robertazzi, A.; Vargiu, A. V.; Gamez, P.; Reedijk, J. *Inorg. Chem.* **2009**, *48*, 5473−5479 and references therein.
(61) Walesa-Chorab, M.; Stefankiewicz, A. R.; Gorczynski, A.; Kubicki, M.; Klak, J.; Korabik, M. J.; Patroniak, V. *Polyhedron* **2011**, *30*, 233−240.
(62) Biswas, C.; Drew, M. G. B.; Asthana, S.; Desplanches, C.; Ghosh, A. *J. Mol. Struct.* **2010**, *965*, 39−44.
(63) Ma, Y.; Cheng, A. L.; Gao, E. Q. *Dalton Trans.* **2010**, *39*, 3521−3526.
(64) Ashcroft, N. W.; Mermin, N. D. *Solid State Physics*; Saunders College Publishing: Philadelphia, 1976.